

A Robotic System for Implant Modification in Single-stage Cranioplasty

Shuya Liu*, Wei-Lun Huang*, Chad Gordon† and Mehran Armand*,†

Abstract—Craniomaxillofacial reconstruction with patient-specific customized craniofacial implants (CCIs) is most commonly performed for large-sized skeletal defects. Because the exact size of skull resection may not be known prior to the surgery, in the single-stage cranioplasty, a large CCI is pre-fabricated and resized intraoperatively with a manual-cutting process provided by a surgeon. The manual resizing, however, may be inaccurate and significantly add to the operating time. This paper introduces a fast and non-contact approach for intraoperatively determining the exact contour of the skull resection and automatically resizing the implant to fit the resection area. Our approach includes four steps: First, a patient’s defect information is acquired by a 3D scanner. Second, the scanned defect is aligned to the CCI by registering the scanned defect to the reconstructed CT model. Third, a cutting toolpath is generated from the contour of the scanned defect. Lastly, the large CCI is resized by a cutting robot to fit the resection area according to the given toolpath. To evaluate the resizing performance of our method, six different resection shapes were used in the cutting experiments. We compared the performance of our method to the performances of surgeon’s manual resizing and an existing technique which collects the defect contour with an optical tracking system and projects the contour on the CCI to guide the manual modification. The results show that our proposed method improves the resizing accuracy by 56% compared to the surgeon’s manual modification and 42% compared to the projection method.

I. INTRODUCTION

Cranioplasty is a procedure to treat cranial defects due to trauma, injury, or neurosurgical procedures for brain tumors, aneurysms or epilepsy [1]. Conventional cranioplasty is a two-stage process that repairs skull deformities in a delayed operation [2]. Such process requires the skull to be partially removed from the patient who then has to wait for the design and fabrication of the replacing implant for three to four weeks. In contrast, single-stage cranioplasty aims to restore aesthetic appearance immediately following craniectomy within one single operation, therefore, decreasing operative times and speeding up the patient’s recovery [3]. In practice, cranioplasty replaces the skull defect with an alloplastic implant instead of using a patient’s autologous skull-bone [4].

* Shuya Liu is with the Department of Mechanical Engineering, Johns Hopkins University, Baltimore, MD. jsliu@jhu.edu

* Weilun Huang is with the Department of Computer Science, Johns Hopkins University, Baltimore, MD. w1.huang@jhu.edu

† Chad Gordon is with the Neuroplastic and Reconstructive Surgery, Johns Hopkins School of Medicine, Baltimore, MD. cgordon@jhmi.edu

*† Mehran Armand is with the Department of Mechanical Engineering, Johns Hopkins University, Baltimore, MD; the Department of Orthopaedic surgery, the Johns Hopkins School of Medicine, Baltimore, MD. marmand2@jhu.edu

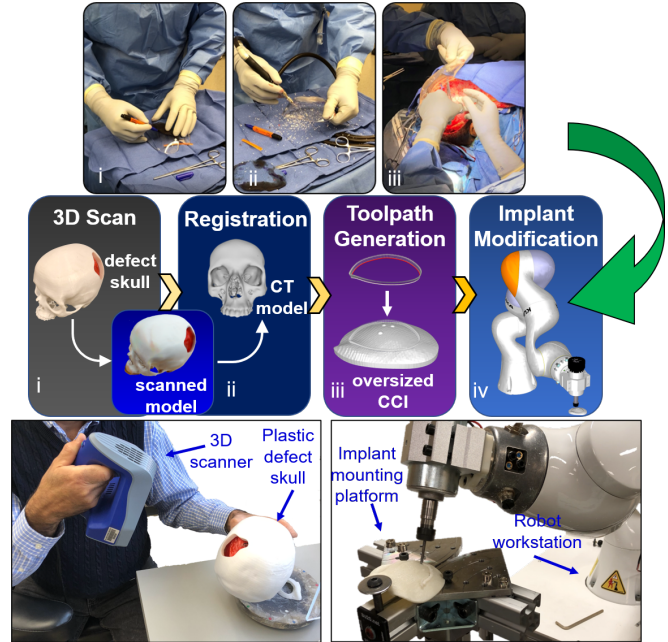


Fig. 1. Top: A clinical example of the single-stage cranioplasty with a prefabricated large CCI. i) the surgeon marks the defect contour on the CCI. ii) the implant is manually modified by a surgical cutter. iii) the resized CCI is placed to the skull defect. Middle: The workflow of robotic single-stage cranioplasty. i) 3D scanning generates a scanned model of the defect skull. ii) the scanned model is registered to its CT model. iii) a cutting toolpath is generated. iv) The implant is resized by the robot. Bottom: Left: The plastic defect skull is scanned by a handheld 3D scanner. Right: robot resizes the oversized implant.

Several approaches are utilized to generate CCIs. Molding technique has been applied to form CCIs in the operating room [5]. This method requires injecting liquid bio-compatible materials such as poly-methyl-methacrylate directly into the defect of the skull or a molding template generated using the autologous bones. However, molding a CCI directly on the defect may release an exothermic reaction damaging nearby tissue [6]. Moreover, autologous bones cannot always be used to create a negative imprint and are limited in their ability to eliminate the discontinuities between the boundaries. Another commonly used approach is a cutting guide, in which a customized implant and a cutting guide are prefabricated and the surgeon resects the patient’s skull along the cutting guide so that skull defect can be immediately closed with the prefabricated CCI [7], [8]. In addition, some other groups considered using optical navigation systems to achieve planned resections. [9], [10]. Although these methods are capable of repairing skull deformities within one operation, they do not consider

the possibilities for intraoperative plan changes, limiting neurosurgeons' flexibility in reaching specific regions of the brain. In [3], [11], a clinical approach using prefabricated large CCIs in single-stage cranioplasty is presented. This approach requires a surgeon to intraoperatively modify an oversized CCI by manually resizing it, which is often poor in accuracy and time-consuming.

Computer-assisted single-stage cranioplasty provides a method to help surgeons better visualize the defect contour by directly projecting the defect contour on an oversized CCI. This method utilizes an optical tracking system to collect data points of the defect contour [12]. However, this system is difficult to set up and requires line-of-sight. Moreover, the planar projection from a fixed configuration may not be suitable for implants with complex structures. To address the above-mentioned problems, we previously developed a portable projection mapping device that tracks surgical instruments and projects a 3D defect contour onto the implant in real-time from any angle without information loss [13]. Although this approach improves the accuracy of projection mapping for medical augmented reality, it can only collect one data point per frame with a digitizing instrument. Therefore, this approach takes longer to collect sufficient data points for registration.

Recent advances in 3D scanning technologies provide new venues for extending the application of medical robots in the operating room [14]. 3D scanning generates high-precision 3D models of real-world objects that can be recognized within a robot's workspace to achieve specific autonomous tasks. Different from the optical tracking system, a 3D scanner can collect thousands of data points per frame without contacting the object. The use of a 3D scanner for skull defect reconstruction can simplify and expedite the identification of the defect's contour.

In this paper, we present a novel system for generating precise CCIs for patients in single-stage cranioplasty. The system consists of a 3D scanner and a cutting robotic arm. The 3D scanning technique enables fast registration and generation of cutting toolpaths. The cutting robotic arm provides stable and accurate performance compared to the manual cutting approach by surgeons. The **contributions** of this work include: 1) We proposed a fast and non-contact approach for acquiring defect contour information using a handheld 3D scanner. 2) We developed an algorithm for generating cutting toolpaths from the extracted defect contours. 3) We integrated a robotic system for automatic implant modification. 4) Our approach improved the accuracy of the implant modification compared to the conventional manual approach and an existing method using an optical tracking system.

II. METHOD

We developed a robotic system for resizing oversized CCIs during intraoperative operation. The system consists of a handheld Artec Space Spider 3D scanner (up to 0.1 mm resolution) and a KUKA LBR iiwa 7 R800 robotic arm. The 3D scanner was utilized to acquire 3D information of the

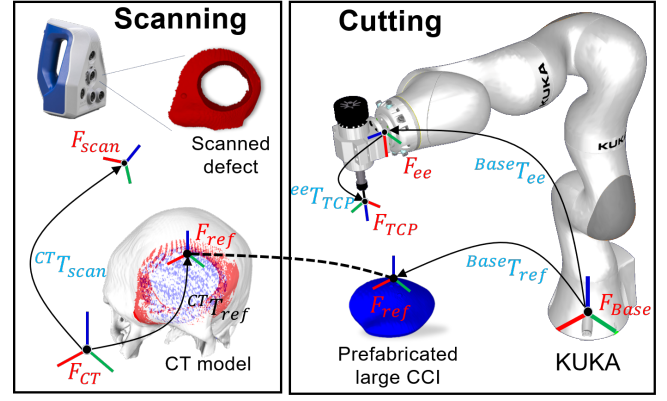


Fig. 2. Coordinate transformations between different models. Left: the 3D scanned defect mesh model in F_{scan} is registered to the CT model in F_{CT} . Right: the bottom (blue) is a prefabricated oversized CCI with a reference frame F_{ref} defined by three spherical markers. F_{Base} is the robot's base frame. F_{ee} is the robot's end-effector frame. F_{TCP} is the frame attached to the calibrated TCP. The transformation between different coordinate frames are shown as T .

skull defect and to export a refined mesh (Fig. 1, bottom, left). The KUKA robotic arm was modified into a cutting workstation by adding a spindle tool to the robot's end-effector (Fig. 1, bottom right).

Our CCI generation method includes four steps (Fig. 1, middle): 1) The information of a defected skull is collected using a 3D scanner. 2) The scanned data is registered to the CT model space. 3) A cutting toolpath is generated by extracting the defect contour. 4) A cutting robot resizes the CCI according to the generated toolpath.

A. 3D reconstruction of a patient's defect skull

A 3D scanning process was first implemented using a handheld 3D scanner. During this process, the 3D scanner was held by hand at an approximate half meter distance from the skull and moved slowly around it. This process could be terminated when there were sufficient 3D point cloud data shown in the visualization software. This process usually takes less than two minutes.

B. Patient-CT registration

The 3D-scanned data was then registered to the preoperative CT model of the patient's skull. This process transformed the scanned data to the CT model space. An iterative closest points (ICP) registration method was applied with an initialization using anatomical points [15]. The anatomical points were selected from the scanned model of the patient.

During the registration process, the 3D-scanned data tends to mistakenly overlap with the inner layer of the skull, because of the similar geometric feature between the inner and outer layer. To prevent this problem, we designed a preprocessing algorithm to remove the CT model's inner layer and to generate a polygon surface model.

In this method, we defined the 3D position of each vertex in the CT skull mesh as $\mathbf{q}_i \in \mathbb{R}^3$. Then the center of the mesh $\mathbf{o} \in \mathbb{R}^3$ can be approximated by: $\mathbf{o} = \frac{\sum_{i=1}^n \mathbf{q}_i}{n}$. Then we constructed vector \mathbf{v}_i , which points from the center \mathbf{o}

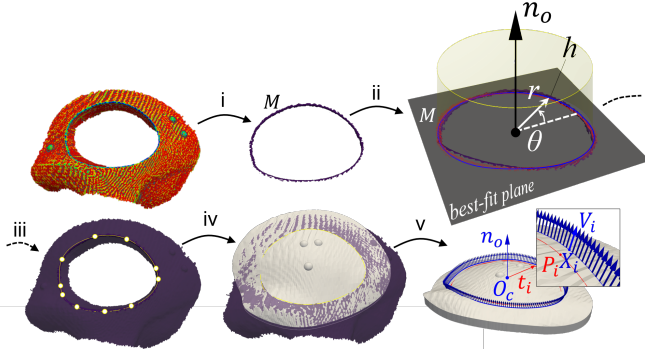


Fig. 3. Toolpath generation. (i) The raw 3D-scanned defect is filtered by curvature. The largest connected component is preserved. (ii) The remaining vertices are fitted to a plane, transformed to a local cylindrical coordinate system defined on the plane parameterized as (θ, r, h) , and then fitted to a polynomial curve. (iii) The fitted curve is turned into a spline interpolated through control points. (iv) The control points are projected onto the implant's top surface. (v) A cutting toolpath is generated from the spline curve.

to each vertex \mathbf{q}_i . Since each vertex in the skull mesh is also associated with a normal vector \mathbf{n}_i of its own. The vectors of the inner layer point to the hollowed space inside the skull towards the center \mathbf{o} , while the vectors of the outer layer point to the opposite directions. As a result, the sign of $\mathbf{q}_i \cdot \mathbf{n}_i$ determines whether this vertex is located in the inner layer or the outer layer. We removed all the vertices with non-positive inner products to ensure that only outer layer of the CT mesh was preserved.

C. Toolpath Generation

To generate a toolpath for resizing process, the defect contour was first extracted from the 3D-scanned mesh of the patient's head. Then, the scanned defect was aligned to the implant by registering the defect to the CT model. A toolpath consisting cutting positions and vectors along the extracted contour was generated in the coordinate frame of the CT model (Fig. 3). We implemented the following steps to generate 3D cutting toolpaths using Pyvista [16]:

1) *Curvature Filter*: To extract the contour of the defect, a curvature filter was applied to the vertices of the scanned mesh and followed by manual adjustments. We utilized a curvature filter to determine the local mean curvature along the surface of the defect and extracted the high curvature value above a designed threshold. The mean curvature H , was calculated as $H = \frac{1}{2}(\kappa_1 + \kappa_2)$, where κ_1 and κ_2 are the maximum and minimum values of the principal curvature on the mesh [17]. This filter was able to identify crease changes in the curvature of the surface. After curvature filtering, only the largest component was kept (Fig. 3, i). Additional manual adjustments could further remove potential redundant vertices that were connected to the largest component.

2) *Curve Fitting*: After removing the redundant vertices, a group of vertices around the defect contour were left denoted as M (Fig. 3, ii). We first defined a local cylindrical coordinate system on a best-fit plane of the extracted contour parameterized as (θ, r, h) . The center of the cylindrical

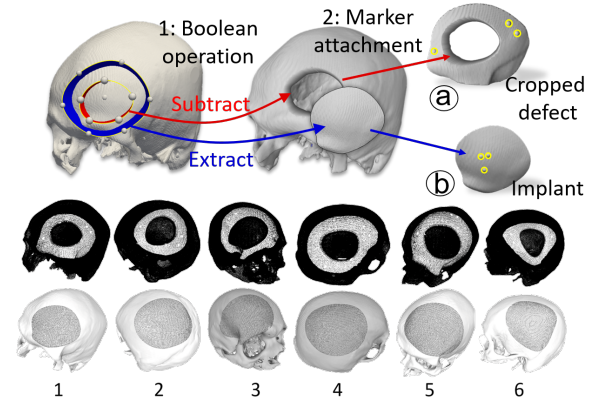


Fig. 4. Implant and skull defect generation. Top: the skull defect (a) and the implant (b) are generated by (1) a boolean operation between the skull and two customized contours (red contour: skull defect, blue contour: implant) and (2) attaching spherical markers to their surfaces. The skull defect is cropped to a 3-D printable size. Bottom: the skull defects (top) and implants (bottom) for six different specimens are generated.

coordinate system was obtained by the mean coordinates of the contour. Then a nonlinear least squares method was used to fit a polynomial expression of the curve.

3) *Spline Projection*: The fitted curve was then converted into a spline, which consists of control points along the fitted curve. Since the oversized implant and defect were already aligned in the CT coordinate system after Patient-CT registration, the control points were projected onto the top surface of the implant. Therefore, the shape of the spline remained consistent with the curvature of the implant (Fig. 3, iv).

4) *Toolpath Generation*: For each discretized point \mathbf{P}_i along the spline curve, a unit 3D vector \mathbf{V}_i was generated to guide tool axis of the cutting path. At first, each \mathbf{V}_i was initialized as \mathbf{n}_o of the best-fit plane. By combining \mathbf{n}_o and each vector \mathbf{t}_i from the center point O_c to each discretized point \mathbf{P}_i , the generated cutting vectors \mathbf{V}_i could be tilted by a cut angle. The obtained vector \mathbf{V}_i were then assigned to each discretized point \mathbf{P}_i to form the toolpath. To compensate the tool radius, the discretized points $\sum \mathbf{P}_i$ could be expanded with an offset equal to the radius of the cutting tool (Fig. 3, v).

III. EXPERIMENTAL SETUP

To evaluate the implant-resizing accuracy of our integrated system, we compared our method with the surgeon's manual-resizing method and an existing optical tracking method. We conducted six experiments with independently generated skull defects with different sizes and shapes using boolean operations. As shown in Fig. 4 (Top), we first subtracted the mesh inside the red contour from a complete skull to create a defect on the skull. On the same complete skull, the implant mesh inside the blue contour was extracted to create its corresponding oversized implant. The defected skull was further cropped to a 3D printable size and was fabricated using a 3-D printer (Stratasys F370, ABS material). Finally, we attached three spherical markers on the top surface

of each cropped defect and its corresponding implant for Patient-CT registration and implant localization (Fig. 2, F_{ref}).

A. Method comparison

We compared the implants generated by our method with manual resizing method, as well as the optical tracking method used by [12]. For robotic cutting, the cut depth was set to 3 mm, which is the same as thickness of the designed implants. The cut angle was set to 20 degrees for all the generated cutting toolpaths.

1) *Manual resizing method:* We provided the surgeon with pre-designed partial skulls with the generated defects and corresponding over-sized implants. The surgeon outlined the defect contour of each specimen manually based on his visual judgment. He then resized the implant with a hand-held cutting tool.

2) *Optical tracking method:* The optical tracking method used a digitizing instrument and an optical tracking system to trace the defect contour (Fig. 5, a). The defect contours were then cut by the same cutting robot and with same cutting parameters described above.

B. Tool Center Point (TCP) Calibration

The transformation between the tip of the spindle tool and the robot arm's end-effector was calibrated using a pivot calibration [18]. In this method, we hand-guided the robotic arm to different poses, such that the TCP always touches the tip of a fixed pin. The accuracy of the TCP calibration, measured by the TCP error, is shown in Fig. 5.

C. Implant Localization

The oversized CCI was secured on the mounting platform with bolts for the resizing process (Fig. 1, bottom, right). In order to obtain the relative position and orientation of the oversized CCI in the robot space (Fig. 2, right), the robot was hand-guided so that the TCP touched the tip of each spherical marker separately.

The transformation between the local reference frame F_{ref} of the oversized CCI and the robot base F_{base} can be then calculated based on the known locations of the markers, described in the F_{ref} , and the relative positions from F_{base} to F_{TCP} :

$${}^{Base}T_{TCP} = {}^{Base}T_{ee} \cdot {}^{ee}T_{TCP}$$

D. Experimental Details

The integrated system was set up on a computer running Intel Core i7-6820HQ @ 2.7GHz CPU. The 3D scanner (Artec Spider) collects data at 15 HZ. The KUKKA robot is operated using online mode via RoboDK¹. The registration between the 3D-scanned model and the CT model was implemented in Meshlab, an open-source software for mesh processing [19]. The NDI Polaris optical tracking system operates at 10 Hz (0.3 mm tracking accuracy) was used in the comparison experiment.

¹RoboDK is an offline programming and simulation software for industrial robots. <https://robodk.com/>

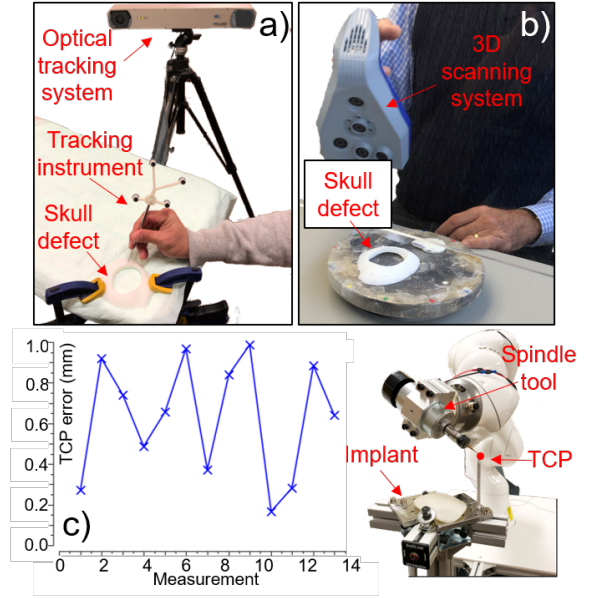


Fig. 5. Top: a) collecting the defect contour by optical tracking system. b) scanning the defect contour with a handheld 3D scanner. c) robot TCP calibration errors

IV. RESULT

A. Registration

1. Registration by optical tracking system

Three anatomical markers were artificially added to the original CT models and were 3D printed with the defect specimens. The anatomical points on the printed specimens were localized in the optical tracking system with a tracking instrument (Fig. 5, a). Then, they were registered back to the CT coordinate system using a singular value decomposition algorithm [20]. The registration error was given by the mean Cartesian distance between the registered anatomical points and the original anatomical points in the CT model (Table I).

2. Registration by 3D scanner

After scanning the defect specimen, we first manually aligned the three anatomical points on the defect with the original anatomical points defined in the CT model as an initialization. Then ICP was used to fine-tune the registration of the scanned specimen to the original CT model. The error was evaluated by calculating the mean distance between all of the registered points and their corresponding points in the original CT model (Table I).

B. Evaluation of resized implants

The post-completed implants were fitted to the defect specimens. They were then 3D scanned and registered to the original CT models using the anatomical points on the defect specimens. Each post-completed implant was then individually scanned by 3D scanner and registered to the previous scan of the implant fitted to the defect, so that the implant can be put to the correct position relative to the ground truth defect.

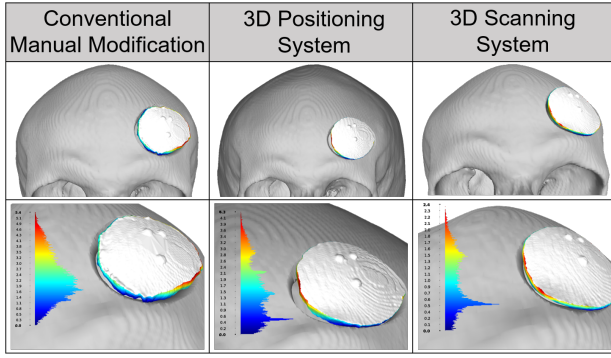


Fig. 6. An example of gap distance analysis (the first specimen). Left, middle, right show the results of conventional manual modification, 3D positioning system, and 3D scanning system, respectively. Top and bottom show their overviews and their zoomed views. The color bars in the bottom plots show the gap distance between the implant's boundary and its fitted defect wall.

We then evaluated the gap distances between the boundaries of the cut implants and their respective defect walls. The gap distances were visualized in Meshlab [19] (Fig. 6). We used the gap distance distribution (maximum, mean and standard deviation) to quantify the error for each method for the 6 specimens (Fig. 7). Among the mentioned three methods, our robot-3d-scan integrated method was the only one with the mean gap distance below 1.5 mm (Fig. 8).

C. Time cost

Not only does our method achieve the best accuracy, it is also comparable in the time it takes to utilize the conventional manual method (Table II), and it would not affect the ongoing surgery time.

TABLE I
REGISTRATION ERRORS OF TWO METHODS

	S1	S2	S3	S4	S5	S6
3D positioning system (mm)	0.39	0.38	0.32	0.32	0.30	0.34
3D scanning system (mm)	0.04	0.02	0.04	0.04	0.05	0.03

TABLE II
TIME SPAN OF TWO METHODS (MINUTES)

	Surgeon	Proposed method	
Data acquisition	1	3D Scan	1
		patient-CT registration	1
		toolpath generation	1
		implant localization	1
Implant modification	4 - 8	robot execution	2 - 3
Total time	5 - 9	6 - 7	

V. DISCUSSION

We present a novel method for intraoperatively fabricating precise CCI in single-stage cranioplasty. In the proposed method, we first scan the defect to create a mesh model. The mesh model is then registered to the reconstructed 3D from

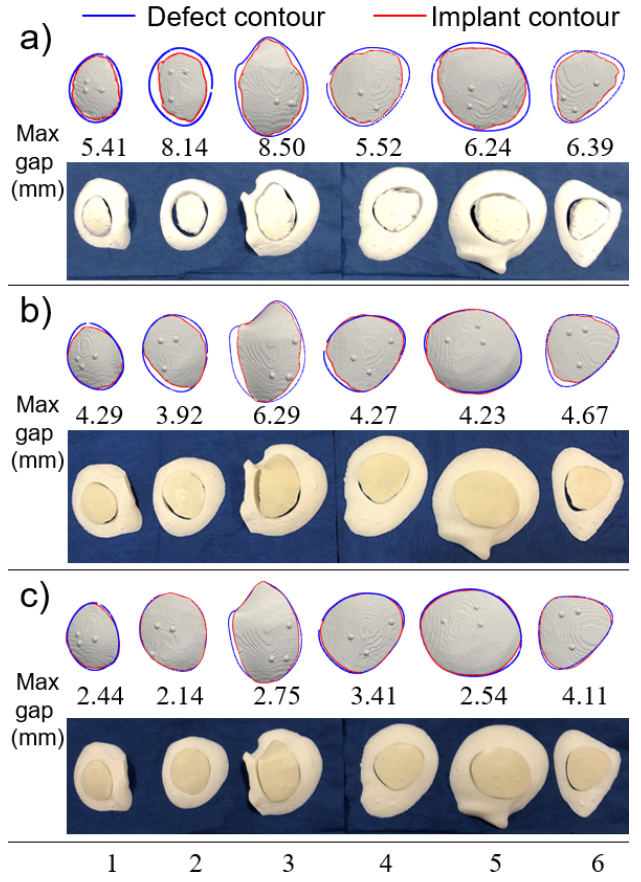


Fig. 7. Cutting performance. Visualization of the defect contour (blue curve) and implant contour (red curve) for a) conventional manual modification, b) 3D positioning system, and c) 3D scanning system. The numbers in the middle of each plot show the maximum gap distance.

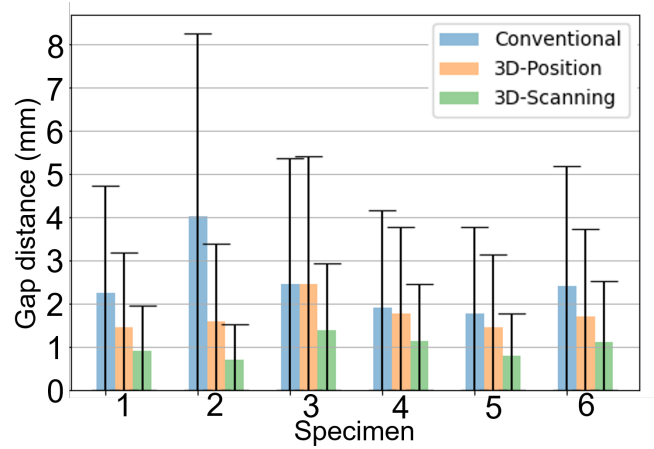


Fig. 8. Cutting accuracy evaluation. Mean and standard deviation of the gap distance between the implant and the defect of conventional manual modification (blue), 3D positioning system (orange), and 3D scanning system (green) for six specimens.

CT data in order to define the contour of the defect. Next, a cutting toolpath is generated using the discretized defect contour. After localizing the oversized CCI in the robot's base frame, an automatic cutting process is implemented to

generate the final CCI implant.

The proposed method improves the accuracy of the cut by 56% compared to the surgeon's cut and 42% compared to the optical tracking method. Moreover, the implant cut boundaries as created by the robot were considerably smoother than those created by the expert surgeon. The smooth boundary may contribute to the better fit of implants to the defect area in actual surgical scenarios. Our proposed method, however, only moderately reduced the operation time compared to the expert surgeon. Of note, the expert surgeon's performance time (5-9 minutes) in this study was significantly below the lower spectrum of 10-80 minutes as reported by Berli et al [3]. The robotic modification of oversized CCIs were shown to be more consistent and accurate when compared to the expert surgeon's performance. Of note, We used an available seven DOF Kuka robot to perform the cutting tasks. However, a cheaper six DOF robot or a five-axis laser cutting machine (e.g. [21]) can also successfully perform smooth cutting as proposed for this research.

Some of the limitations of the current study are as follows: 1) During the toolpath generation process, the cut angle defining the tool axis attached to the discretized points along the defect contour were constant. In actual surgical scenarios, This may cause problems in fitting the implant if the defect boundary is not beveled uniformly. The extension of this work will include the development of an algorithm that can extract the bevel angle of the defect wall from the scan data. 2) In this study, the manually-tuned, experimentally-determined cutting speed and spinning rate of the tool were not optimized. Additional experiments are needed to evaluate the optimal cutting parameters for smooth cutting of the implant. 3) In the clinical setting, due to the minimally exposed surgical area (Figure 1, Top, iii), the process of registering a patient's defect scan to the CT model may be challenging. A possible remedy is to use two separate 3D scans at different times during the procedure. Prior to draping of the patient, marks will be drawn within the surgical area. The first scan will acquire the full exposed head as well as the drawn marks and register this head model to the preoperative CT scan of the patient's skull. After draping the surgical area and subsequent skull resection, a second scan containing the defect area information will be registered to the first scan using the information obtained from the drawn marks. Thereby, the defect scan can be mapped to the CT model through the intermediate scan obtained prior to draping.

REFERENCES

- [1] S. Aydin, B. Kucukyuruk, B. Abuzayed, S. Aydin, and G. Z. Sanus, "Cranioplasty: review of materials and techniques," *Journal of neurosciences in rural practice*, vol. 2, no. 2, p. 162, 2011.
- [2] C. M. Pasick, K. Margetis, G. F. Santiago, C. Gordon, and P. J. Taub, "Adult cranioplasty," *Journal of Craniofacial Surgery*, vol. 30, no. 7, pp. 2138–2143, 2019.
- [3] J. U. Berli, L. Thomaier, S. Zhong, J. Huang, A. Quinones, M. Lim, J. Weingart, H. Brem, and C. R. Gordon, "Immediate single-stage cranioplasty following calvarial resection for benign and malignant skull neoplasms using customized craniofacial implants," *Journal of Craniofacial Surgery*, vol. 26, no. 5, pp. 1456–1462, 2015.
- [4] A. M. Shah, H. Jung, and S. Skirboll, "Materials used in cranioplasty: a history and analysis," *Neurosurgical focus*, vol. 36, no. 4, p. E19, 2014.
- [5] A.-R. Fathi, S. Marbacher, and A. Lukes, "Cost-effective patient-specific intraoperative molded cranioplasty," *Journal of craniofacial surgery*, vol. 19, no. 3, pp. 777–781, 2008.
- [6] S. Marbacher, L. Anderegg, S. Erhardt, A.-R. Fathi, J. Fandino, A. Raabe, and J. Beck, "Intraoperative template-molded bone flap reconstruction for patient-specific cranioplasty," *Neurosurgical review*, vol. 35, no. 4, pp. 527–535, 2012.
- [7] H. Eufinger, A. R. Wittkamp, M. Wehmöller, and F. W. Zonneveld, "Single-step fronto-orbital resection and reconstruction with individual resection template and corresponding titanium implant: a new method of computer-aided surgery," *Journal of Cranio-Maxillofacial Surgery*, vol. 26, no. 6, pp. 373–378, 1998.
- [8] G. Gerbino, F. A. Bianchi, E. Zavattero, F. Tartara, D. Garbossa, and A. Ducati, "Single-step resection and reconstruction using patient-specific implants in the treatment of benign cranio-orbital tumors," *Journal of Oral and Maxillofacial Surgery*, vol. 71, no. 11, pp. 1969–1982, 2013.
- [9] F. Jalbert, S. Boetto, F. Nadon, F. Lauwers, E. Schmidt, and R. Lopez, "One-step primary reconstruction for complex craniofacial resection with peek custom-made implants," *Journal of Cranio-Maxillofacial Surgery*, vol. 42, no. 2, pp. 141–148, 2014.
- [10] P. Dodier, F. Winter, T. Auzinger, G. Mistelbauer, J. M. Frischer, W.-T. Wang, A. Mallouhi, W. Marik, S. Wolfsberger, L. Reissig et al., "Single-stage bone resection and cranioplastic reconstruction: comparison of a novel software-derived peek workflow with the standard reconstructive method," *International journal of oral and maxillofacial surgery*, vol. 49, no. 8, pp. 1007–1015, 2020.
- [11] A. Wolff, G. F. Santiago, M. Belzberg, C. Huggins, M. Lim, J. Weingart, W. Anderson, A. Coon, J. Huang, H. Brem et al., "Adult cranioplasty reconstruction with customized cranial implants: preferred technique, timing, and biomaterials," *Journal of Craniofacial Surgery*, vol. 29, no. 4, pp. 887–894, 2018.
- [12] R. J. Murphy, K. C. Wolfe, P. C. Liacouras, G. T. Grant, C. R. Gordon, and M. Armand, "Computer-assisted single-stage cranioplasty," in *2015 37th Annual International Conference of the IEEE Engineering in Medicine and Biology Society (EMBC)*. IEEE, 2015, pp. 4910–4913.
- [13] S. Liu, W.-L. Huang, A. Shin, C. Gordon, and M. Armand, "A portable projection mapping device for medical augmented reality in single-stage cranioplasty," in *Optical Architectures for Displays and Sensing in Augmented, Virtual, and Mixed Reality (AR, VR, MR)*, vol. 11310. International Society for Optics and Photonics, 2020, p. 1131007.
- [14] A. Haleem and M. Javaid, "3d scanning applications in medical field: a literature-based review," *Clinical Epidemiology and Global Health*, vol. 7, no. 2, pp. 199–210, 2019.
- [15] P. J. Besl and N. D. McKay, "Method for registration of 3-d shapes," in *Sensor fusion IV: control paradigms and data structures*, vol. 1611. International Society for Optics and Photonics, 1992, pp. 586–606.
- [16] C. B. Sullivan and A. A. Kaszynski, "Pyvista: 3d plotting and mesh analysis through a streamlined interface for the visualization toolkit (vtk)," *Journal of Open Source Software*, vol. 4, no. 37, p. 1450, 2019.
- [17] M. Meyer, M. Desbrun, P. Schröder, and A. H. Barr, "Discrete differential-geometry operators for triangulated 2-manifolds," in *Visualization and mathematics III*. Springer, 2003, pp. 35–57.
- [18] W. Birkfellner, F. Watzinger, F. Wanschitz, R. Ewers, and H. Bergmann, "Calibration of tracking systems in a surgical environment," *IEEE transactions on medical imaging*, vol. 17, no. 5, pp. 737–742, 1998.
- [19] P. Cignoni, M. Callieri, M. Corsini, M. Dellepiane, F. Ganovelli, and G. Ranzuglia, "Meshlab: an open-source mesh processing tool," in *Eurographics Italian chapter conference*, vol. 2008. Salerno, 2008, pp. 129–136.
- [20] K. S. Arun, T. S. Huang, and S. D. Blostein, "Least-squares fitting of two 3-d point sets," *IEEE Transactions on pattern analysis and machine intelligence*, no. 5, pp. 698–700, 1987.
- [21] J. Liu, J. Fang, R. J. Murphy, C. Gordon, and M. Armand, "Design and development of 5-axis cranial implant laser cutting system," in *International Design Engineering Technical Conferences and Computers and Information in Engineering Conference*, vol. 58110. American Society of Mechanical Engineers, 2017, p. V001T02A051.